Finally, Fig. 3 presents an expanded view of the low-temperature region. Here, the experimental unitary data are calibrated and replotted in the more conventional theoretical units, $E_F = k_B T_F$ and T_F. The agreement between theory and experiment is very good. In the presence of a pseudogap, a more elaborate treatment (*28*) of the pseudogap self energy, which takes into account spectral broadening, will be needed in order to calculate accurately the jump in specific heat.

By extending the temperature range in Fig. 3 to high T, we find that both the unitary and noninteracting cases coincide above a characteristic temperature, T^*, although below T_c they start out with different power laws (as shown in Fig. 2). In general, we find that agreement between theory and experiment is very good over the full temperature range for which the data were taken. The observation that the interacting and noninteracting curves do not precisely coincide until temperatures rise substantially above T_c is consistent with (although it does not prove) the existence of a pseudogap and with onset temperature from the figure $T \approx 2\ T_c$. Related signatures of pseudogap effects are also seen in the thermodynamics of high-temperature superconductors (*17*).

References and Notes

1. K. M. O'Hara, S. L. Hemmer, M. E. Gehm, S. R. Granade, J. E. Thomas, *Science* **298**, 2179 (2002).
2. J. E. Thomas, M. E. Gehm, *Am. Sci.* **92**, 238 (2004).
3. H. Heiselberg, *Phys. Rev. A.* **63**, 043606 (2001).
4. T.-L. Ho, *Phys. Rev. Lett.* **92**, 090402 (2004).
5. J. G. A. Baker, *Phys. Rev. C* **60**, 054311 (1999).
6. J. Carlson, S.-Y. Chang, V. R. Pandharipande, K. E. Schmidt, *Phys. Rev. Lett.* **91**, 050401 (2003).
7. A. Perali, P. Pieri, G. C. Strinati, *Phys. Rev. Lett.* **93**, 100404 (2004).
8. M. E. Gehm, S. L. Hemmer, S. R. Granade, K. M. O'Hara, J. E. Thomas, *Phys. Rev. A* **68**, 011401(R) (2003).
9. T. Bourdel *et al.*, *Phys. Rev. Lett.* **93**, 050401 (2004).
10. M. Bartenstein *et al.*, *Phys. Rev. Lett.* **92**, 120401 (2004).
11. M. Houbiers *et al.*, *Phys. Rev. A.* **56**, 4864 (1997).
12. R. Combescot, *Phys. Rev. Lett.* **83**, 3766 (1999).
13. M. Holland, S. J. J. M. F. Kokkelmans, M. L. Chiofalo, R. Walser, *Phys. Rev. Lett.* **87**, 120406 (2001).
14. E. Timmermans, K. Furuya, P. W. Milonni, A. K. Kerman, *Phys. Lett. A* **285**, 228 (2001).
15. Y. Ohashi, A. Griffin, *Phys. Rev. Lett.* **89**, 130402 (2002).
16. J. Stajic *et al.*, *Phys. Rev. A.* **69**, 063610 (2004).
17. Q. J. Chen, J. Stajic, S. Tan, K. Levin, available at http://arxiv.org/abs/cond-mat/0404274.
18. C. A. Regal, M. Greiner, D. S. Jin, *Phys. Rev. Lett.* **92**, 040403 (2004).
19. M. W. Zwierlein *et al.*, *Phys. Rev. Lett.* **92**, 120403 (2004).
20. C. Chin *et al.*, *Science* **305**, 1128 (2004).
21. J. Kinast, S. L. Hemmer, M. E. Gehm, A. Turlapov, J. E. Thomas, *Phys. Rev. Lett.* **92**, 150402 (2004).
22. M. Bartenstein *et al.*, *Phys. Rev. Lett.* **92**, 203201 (2004).
23. J. Kinast, A. Turlapov, J. E. Thomas, *Phys. Rev. A* **70**, 051401(R) (2004).
24. F. London, *Phys. Rev.* **54**, 947 (1938).
25. J. Kinast, A. Turlapov, J. E. Thomas, available at http://arxiv.org/abs/cond-mat/0409283.
26. Materials and methods are available as supporting material on *Science* Online.
27. Q. J. Chen, J. Stajic, K. Levin, available at http://arxiv.org/abs/cond-mat/0411090.
28. Q. J. Chen, K. Levin, I. Kosztin, *Phys. Rev. B* **63**, 184519 (2001).
29. A. J. Leggett, *Modern Trends in the Theory of Condensed Matter* (Springer-Verlag, Berlin, 1980), pp. 13–27.
30. J. Kinnunen, M. Rodríguez, P. Törmä, *Science* **305**, 1131 (2004).
31. L. D. Carr, G. V. Shlyapnikov, Y. Castin, *Phys. Rev. Lett.* **92**, 150404 (2004).
32. J. E. Williams, N. Nygaard, C. W. Clark, *N. J. Phys.* **6**, 123 (2004).
33. S. Stringari, *Europhys. Lett.* **65**, 749 (2004).
34. H. Hu, A. Minguzzi, X.-J. Liu, M. P. Tosi, *Phys. Rev. Lett.* **93**, 190403 (2004).
35. H. Heiselberg, *Phys. Rev. Lett.* **93**, 040402 (2004).
36. J. Stajic, Q. J. Chen, K. Levin, available at http://arxiv.org/abs/cond-mat/0408104.
37. C. Menotti, P. Pedri, S. Stringari, *Phys. Rev. Lett.* **89**, 250402 (2002).
38. B. Jackson, P. Pedri, S. Stringari, *Europhys. Lett.* **67**, 524 (2004).
39. M. Bartenstein *et al.*, available at http://arxiv.org/abs/cond-mat/0408673.

40. We thank T.-L. Ho, N. Nygaard, C. Chin, M. Zwierlein, M. Greiner, and D. S. Jin for stimulating correspondence. This research is supported by the Chemical Sciences, Geosciences, and Biosciences Division of the Office of Basic Energy Sciences, Office of Science, U.S. Department of Energy (DOE); the Physics Divisions of the Army Research Office; and NSF, the Fundamental Physics in Microgravity Research program of NASA, NSF-MRSEC grant DMR-0213745; and in part by the Institute for Theoretical Sciences, a joint institute of Notre Dame University and Argonne National Laboratory, and by the U.S. DOE, Office of Science through contract W-31-109-ENG-38.

Supporting Online Material

www.sciencemag.org/cgi/content/full/1109220/DC1
Materials and Methods
Figs. S1 and S2
References and Notes

28 December 2004; accepted 16 January 2005
Published online 27 January 2005;
10.1126/science.1109220
Include this information when citing this paper.

Simultaneous State Measurement of Coupled Josephson Phase Qubits

R. McDermott,[1,2] R. W. Simmonds,[2] Matthias Steffen,[1] K. B. Cooper,[1] K. Cicak,[2] K. D. Osborn,[2] Seongshik Oh,[2] D. P. Pappas,[2] John M. Martinis[1]*

One of the many challenges of building a scalable quantum computer is single-shot measurement of all the quantum bits (qubits). We have used simultaneous single-shot measurement of coupled Josephson phase qubits to directly probe interaction of the qubits in the time domain. The concept of measurement crosstalk is introduced, and we show that its effects are minimized by careful adjustment of the timing of the measurements. We observe the antiphase oscillation of the two-qubit $|01\rangle$ and $|10\rangle$ states, consistent with quantum mechanical entanglement of these states, thereby opening the possibility for full characterization of multiqubit gates and elementary quantum algorithms.

Considerable progress has been made toward the implementation of a quantum computer (*1*) based on superconductors. Coherent single-qubit operations have been shown in Josephson flux (*2*) and phase (*3*) qubits, and the time domain interaction of coupled qubits (*4*) and a controlled-NOT logic gate (*5*) have been demonstrated in the Josephson charge qubit (*6*, *7*). Previous studies of coupled superconducting qubits have relied on separate measurements of the individual qubits (bitwise readout). Such an approach does not yield complete information about the system and fails, for example, to directly establish correlations between the qubits in the case of an entangled state. To test quantum algorithms efficiently or to perform quantum state tomography and thereby definitively prove entanglement, it is necessary to measure all the qubits simultaneously (wordwise readout) and with high fidelity. For multiqubit circuits with fixed coupling—a common architecture for superconducting qubits—the realization of this goal is complicated by measurement crosstalk: Measurement of the state of one qubit may perturb the state of other qubits, destroying information about quantum correlations. Although continued progress toward the realization of quantum gates in superconducting circuits requires a thorough understanding of measurement crosstalk, this issue has received little attention to date.

We describe simultaneous single-shot state measurements to probe the interaction of coupled Josephson phase qubits in the time domain. The observed antiphase oscillation of the occupation probabilities of the two-qubit basis states $|01\rangle$ and $|10\rangle$ is consistent with quantum mechanical entanglement of these

[1]Department of Physics, University of California, Santa Barbara, CA 93106, USA. [2]National Institute of Standards and Technology, 325 Broadway, Boulder, CO 80305, USA.

*To whom correspondence should be addressed. E-mail: martinis@physics.ucsb.edu

states. Moreover, the free evolution between the $|01\rangle$ and $|10\rangle$ states contains the essential ingredient of the two-qubit imaginary-SWAP (*i*-SWAP) operation, which, taken together with single-qubit rotations, forms a universal set of quantum gates (*8*). Our results depend crucially on a scheme for fast (~1 ns) state measurement and accurate adjustment of the timing of the measurements of the two qubits in order to circumvent measurement crosstalk in the circuit. The characteristic decay time for the two-qubit oscillations is consistent with the longitudinal relaxation time of the single-qubit circuit, which suggests that little additional dissipation is introduced by coupling the qubits. This bodes well for future tests of multiqubit gates and for more rigorous demonstrations of quantum correlations in multiqubit circuits.

The Josephson qubit can be thought of as a manufactured electrical "atom" having discrete energy levels that exist in a potential energy landscape determined by the circuit design parameters and bias (Fig. 1, A and B). We previously demonstrated high-resolution spectroscopy and coherent oscillations in the time domain in a single-qubit circuit (*9*, *10*). To implement a coupled qubit circuit, we connected two flux-biased phase qubits via a thin-film capacitor (*11*) (Fig. 1C). We label the qubits A and B. The interaction Hamiltonian can be written

$$H_{\mathrm{int}} = S/2\ (|01\rangle\langle 10| + |10\rangle\langle 01|) \qquad (1)$$

where $|01\rangle \equiv |0_A 1_B\rangle$. In terms of the circuit parameters, the coupling strength is $S \approx (C_x/C_j)\hbar\omega_{10}$, where C_x is the coupling capacitance, C_j is the junction self-capacitance, $\hbar$ is Planck's constant divided by 2π, and ω_{10} is the resonance frequency of the qubits. The interaction can be controlled by adjusting the flux bias of the qubits to change ω_{10}, bringing the qubits in and out of resonance. When the qubits are tuned to resonance (Fig. 2A, inset), the eigenstates are the (entangled) symmetric and antisymmetric combinations of $|01\rangle$ and $|10\rangle$, with eigenenergies $-S/2$ and $S/2$, respectively. Far from resonance, the system behaves as two independent qubits.

Because our circuit is a manufactured quantum system, the energy levels are not known a priori; therefore, we must use spectroscopy to map out the qubit resonance frequencies versus bias (*12*). In the frequency domain, the interaction is manifested as an avoided level crossing at the point where the resonance frequencies of the two qubits are matched (*13*). We biased qubit A to yield a resonance frequency $\omega_{10A}/2\pi$ of 8.65 GHz (*14*). Subsequent spectroscopy of qubit B revealed a splitting S/h = 80 MHz centered at 8.65 GHz (*15*). The measured splitting is consistent with the estimated coupling capacitance and junction self-capacitance of 6 fF and 700 fF, respectively, which are close to the design values.

We next investigated the interaction of the two qubits in the time domain. The qubits were tuned into resonance and initialized in the ground state $|00\rangle$. We then applied an 8.65-GHz microwave π pulse to qubit A to prepare the state $|10\rangle$ (Fig. 2A, inset). Because this state is not an eigenstate of the two-qubit Hamiltonian, it undergoes free evolution in the subspace spanned by the vectors $|01\rangle$ and $|10\rangle$, according to the relation

$$|\Psi(t)\rangle = \tfrac{1}{2}(|10\rangle + |01\rangle)\exp[(iS/2\hbar)t] + \tfrac{1}{2}(|10\rangle - |01\rangle)\exp[-(iS/2\hbar)t] = \cos[(S/2\hbar)t]|10\rangle + i\sin[(S/2\hbar)t]|01\rangle \qquad (2)$$

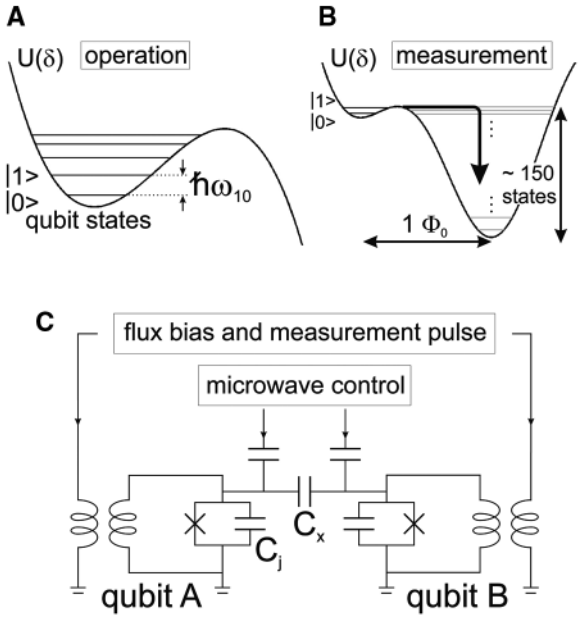

Fig. 1. (**A** and **B**) Potential energy landscape for the flux-biased Josephson phase qubit. During operation, the qubit is biased so that the junction phase δ is trapped in a metastable minimum of the potential $U(\delta)$, which contains several discrete energy levels. Measurement is accomplished by a fast flux pulse that adiabatically lowers the potential barrier, inducing a tunneling transition from the $|1\rangle$ state to the right-hand well of the potential, which contains around 150 states, resulting in a flux change of $\sim 1\Phi_0 \equiv h/2e$. (**C**) Circuit diagram of the coupled phase qubit circuit. The qubit junctions, with self-capacitance $C_j \approx 700$ fF, are coupled via the capacitance $C_x \approx 6$ fF; the junction critical currents are 1.7 μA, and the qubit loop inductances are 720 pH. The qubits are capacitively coupled to the microwave control lines; each qubit loop is inductively coupled to a coil that provides both the flux bias and the measurement pulse, as well as to a dc superconducting quantum interference device (SQUID; not shown) that is used to read out the flux state of the qubit loop. The devices are fabricated from Al/AlOx/Al trilayers by means of conventional thin-film techniques and optical lithography.

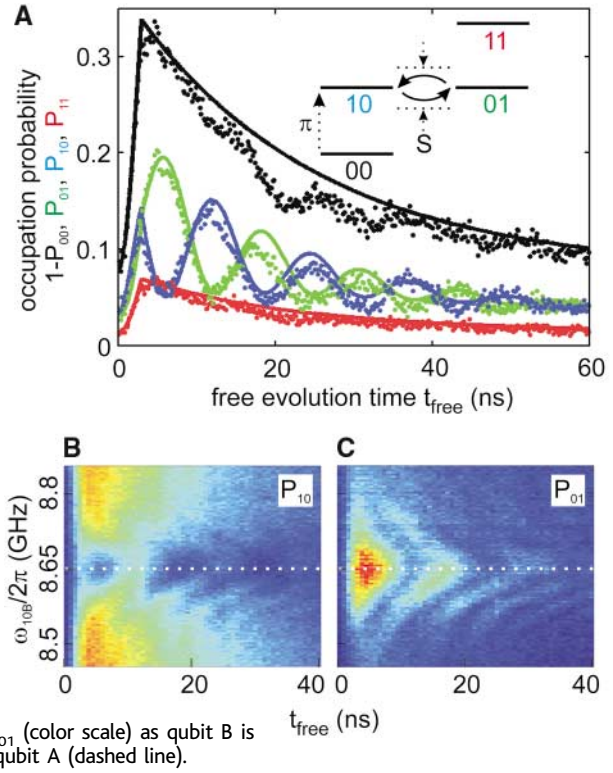

Fig. 2. Interaction of coupled qubits in the time domain. (**A**) With the qubits tuned to resonance $\omega_{10A}/2\pi = \omega_{10B}/2\pi$ = 8.65 GHz, a microwave π pulse on qubit A prepares the state $|10\rangle$. This state subsequently undergoes free precession in the subspace spanned by $|10\rangle$ and $|01\rangle$ before being measured, yielding the state $|00\rangle$, $|10\rangle$, $|01\rangle$, or $|11\rangle$. Repeated measurements give probabilities $1 - P_{00}$, P_{10}, P_{01}, and P_{11}, which are plotted (points) versus free precession time t_{free}. The solid lines are from numerical simulations that assume a gating time of 5 ns for the π pulse and take into account microwave cross-coupling of –10 dB, measurement fidelity of 70%, and a single-qubit T_1 of 25 ns, all determined experimentally from separate measurements. Inset shows the qubit energy levels and depicts schematically the coupling between the states $|10\rangle$ and $|01\rangle$. (**B** and **C**) Oscillations of P_{10} and P_{01} (color scale) as qubit B is detuned from the resonance of qubit A (dashed line).

Therefore, measurements of the two qubits should be anticorrelated, with a $|0\rangle$ for qubit A yielding a measurement of $|1\rangle$ for qubit B and a $|1\rangle$ for qubit A yielding a measurement of $|0\rangle$ for qubit B. After a variable period of free evolution t_{free}, we applied simultaneous measurement pulses to the two qubits, yielding four possible measurement outcomes. By repeated trials (100,000 events per data point), we obtained the occupation probabilities P_{00}, P_{01}, P_{10}, and P_{11}. These probabilities (points) are plotted in Fig. 2A versus t_{free}.

The occupation probabilities P_{01} and P_{10} oscillate out of phase, in agreement with the expected anticorrelation of the states of the two qubits. Moreover, the oscillation period is consistent with the 80-MHz splitting observed in the spectroscopy of the coupled qubits. The reduced amplitude of the oscillations is consistent with simulations (solid lines) that account for a gating time of 5 ns for the π pulse, a measured microwave cross-coupling from qubit A to qubit B of –10 dB, a measured 70% fidelity of the qubit state measurement (*10*), and a measured energy relaxation time T_1 of 25 ns for the individual qubits.

We next repeated the above experiment for a range of qubit detunings by adjusting the flux bias of qubit B. The occupation probabilities P_{01} and P_{10} as functions of both t_{free} and $\omega_{10B}/2\pi$ are shown in Fig. 2, B and C. The oscillation frequency increases and visibility decreases with detuning, resulting in a characteristic "chevron" pattern for the damped oscillations, in agreement with theoretical predictions (*10*).

We emphasize that the antiphase oscillation of the occupations of the $|01\rangle$ and $|10\rangle$ states is most clearly seen when the timing of the measurement pulses is adjusted to ensure simultaneity. As the relative delay t_{delay} of the measurement pulses is increased beyond ~2 ns, we observe a striking change in the character of the evolution of the occupation probabilities (Fig. 3). In the case of sequential measurements of the two qubits, measurement of the $|0\rangle$ state in the first qubit has no effect on the outcome of measurement of the second qubit. On the other hand, measurement of the $|1\rangle$ state in the first qubit results in an enhancement of the probability of measuring the $|1\rangle$ state in the second qubit. We refer to this phenomenon as measurement crosstalk.

The physical mechanism for measurement crosstalk in our circuit can be described as follows. The measurement of a $|1\rangle$ state in the first qubit implies a tunneling event to the right-hand well of the qubit potential. The resulting oscillation in the right-hand well produces a microwave voltage pulse (from the ac Josephson relation). This voltage drives a transient current $I_x(t)$ to the second qubit and induces transitions from the ground state. Because the qubits are weakly coupled ($C_x \ll C_j$), the effect of the current $I_x(t)$ can be understood by treating it as a classical drive to the second qubit. Numerical simulations indicate that the ring up of the second qubit can be separated into three segments in time (Fig. 4, A and B). In segment I, the initial oscillation in the right-hand well of the measured qubit samples the region near the turning point at the top of the well, corresponding to frequencies below

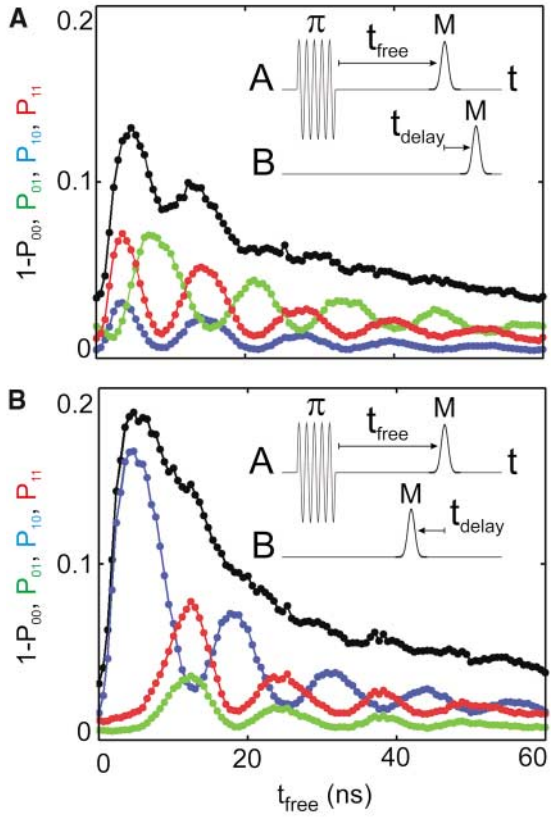

Fig. 3. Measurement crosstalk in the phase qubit, determined by sequential measurement of the states of the qubits. (**A**) Qubit A was measured 4 ns before qubit B; the data are plotted as in Fig. 2. (**B**) Same as (A) but with qubit A measured 4 ns after qubit B. The insets represent the currents applied to each of the qubit junctions; the microwave π pulse prepares the state $|10\rangle$ and Gaussian pulses (labeled *M*) measure the qubit states. When qubit A is measured before qubit B, the oscillations in P_{11} are correlated with the oscillations in P_{10}; when qubit A is measured after qubit B, the oscillations in P_{11} are correlated with the oscillations in P_{01}. From the relative amplitude of the oscillations, we conclude that measurement of $|1\rangle$ in the first qubit results in false measurement of $|1\rangle$ in the second qubit with ~70% probability.

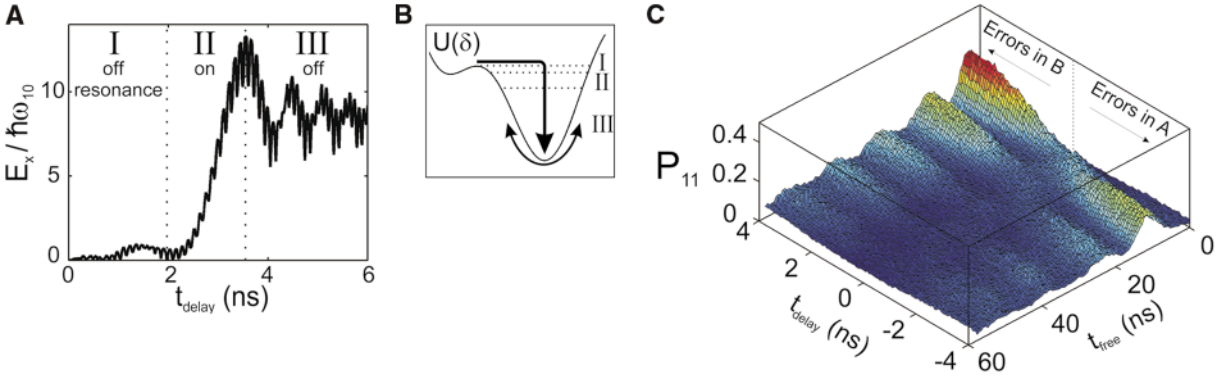

Fig. 4. Description of simultaneous measurement. (**A**) Numerical simulation of the energy transfer to qubit B induced by a tunneling event in qubit A. (**B**) The three stages of energy transfer correspond to energy decay through regions I to III in the potential diagram. (**C**) P_{11} versus free evolution time t_{free} and relative delay t_{delay} of the measurements of the two qubits.

the resonance frequency of the second qubit. The resulting drive current is off resonance with the second qubit; therefore, no appreciable coupling occurs for a time $\sim 0.1T_1$. In segment II, as the oscillations damp and come into resonance with the second qubit, the energy transferred to the second qubit is roughly quadratic in time and can be parameterized as $E_x/\hbar\omega_{10} \sim 10(C_x/C_j)^2[\omega_{10}(t_{delay} - 0.1T_1)]^2$. In segment III, as the measured qubit continues to decay and begins to sample the deepest harmonic regions of the right-hand well, the oscillation frequency moves above the resonance frequency of the second qubit. No additional energy is added, and the energy transferred to the second qubit levels out at a value $E_x/\hbar\omega_{10} \sim 100(C_x/C_j)^2\omega_{10}T_1$. Taking the probability for an $|0\rangle \rightarrow |1\rangle$ transition to be $P_1 \approx E_x/\hbar\omega_{10}$ for $E_x/\hbar\omega_{10} \ll 1$, we predict minimal measurement crosstalk for our circuit for $|t_{delay}| <$ 2 ns. Moreover, we note that the constraint on measurement timing becomes less stringent for qubits with longer T_1.

We investigated the dependence of measurement crosstalk on the timing of the measurements by repeating the experiment of Fig. 2 while varying t_{delay} to cover a total range of ±4 ns (Fig. 4C). When $t_{delay} > 2$ ns, the probability P_{11} is correlated with P_{10}; when $t_{delay} < 2$ ns, P_{11} is correlated with P_{01}. It is only when the relative delay of the measurements is optimally adjusted ($|t_{delay}| <$ 2 ns) that P_{11} is small and the oscillations in P_{11} disappear. Separate experiments indicate that when the timing of the measurement pulses is optimized, a tunneling event in one qubit results in a false measurement of $|1\rangle$ in the second qubit with only 15% probability. This residual measurement crosstalk can be attributed to the finite duration of the measurement pulse.

Our results suggest that it is possible in principle to perform high-fidelity measurements of multiple qubits. Such a technique may lead to scalable quantum information processing based on Josephson junctions.

References and Notes

1. M. A. Nielsen, I. L. Chuang, *Quantum Computation and Quantum Information* (Cambridge Univ. Press, Cambridge, 2000).
2. I. Chiorescu, Y. Nakamura, C. J. P. M. Harmans, J. E. Mooij, *Science* **299**, 1869 (2003); published online 13 February 2003 (10.1126/science.1081045).
3. J. M. Martinis, S. Nam, J. Aumentado, C. Urbina, *Phys. Rev. Lett.* **89**, 117901 (2002).
4. Yu. A. Pashkin *et al.*, *Nature* **421**, 823 (2003).
5. T. Yamamoto, Yu. A. Pashkin, O. Astafiev, Y. Nakamura, J. S. Tsai, *Nature* **425**, 941 (2003).
6. Y. Nakamura, Yu. A. Pashkin, J. S. Tsai, *Nature* **398**, 786 (1999).
7. D. Vion *et al.*, *Science* **296**, 886 (2002).
8. J. Kempe, K. B. Whaley, *Phys. Rev. A* **65**, 052330 (2002).
9. R. W. Simmonds, K. M. Lang, D. A. Hite, D. P. Pappas, J. M. Martinis, *Phys. Rev. Lett.* **93**, 077003 (2004).
10. K. B. Cooper *et al.*, *Phys. Rev. Lett.* **93**, 180401 (2004).
11. P. R. Johnson *et al.*, *Phys. Rev. B* **67**, 020509 (2003).
12. J. M. Martinis, M. H. Devoret, J. Clarke, *Phys. Rev. Lett.* **55**, 1543 (1985).
13. A. J. Berkley *et al.*, *Science* **300**, 1548 (2003); published online 15 May 2003 (10.1126/science.1084528).
14. At this frequency, the spectra of both qubits were free of fine structure normally attributed to spurious junction resonances (*9*).
15. R. McDermott *et al.*, data not shown.

16. Supported in part by the National Security Agency (NSA) Advanced Research and Development Activity (ARDA) through Army Research Office grants W911NF-04-1-2004 and MOD717304.

16 November 2004; accepted 6 January 2005
10.1126/science.1107572

Evidence for a Great Medieval Earthquake (~1100 A.D.) in the Central Himalayas, Nepal

J. Lavé,[1]*† D. Yule,[2]* S. Sapkota,[3] K. Basant,[3] C. Madden,[4] M. Attal,[1] R. Pandey[3]

The Himalayan orogen has produced three thrust earthquakes with moment magnitude (M_w) 7.8 to 8.5 during the past century, yet no surface ruptures associated with these great earthquakes have been documented. Here, we present paleoseismic evidence from east central Nepal that, since ~700 A.D., a single earthquake ruptured the Frontal Thrust fault at ~1100 A.D., with a surface displacement of ~17 (+5/–3) meters and a lateral extent and size that could have exceeded 240 kilometers and ~M_w 8.8, respectively. Ruptures associated with M_w <8.2 events would contribute to the frontal Himalayas folding but would stop before reaching the surface. These findings could require substantial modifications to current regional seismic hazard models.

The primary features of the Himalayan orogen are now understood, but the details of its seismotectonic behavior and maximum earthquake magnitudes are mostly unknown, despite their important implications regarding the seismic hazards facing densely populated regions. During the past century, the Himalayan arc has experienced three major thrust earthquakes of moment magnitude (M_w) >7.8. Growth folding (*1*, *2*) and surface faulting (*3*–*5*) have been reported in Holocene strata and terraces; paradoxically, none of these recent events reportedly produced coseismic surface ruptures, including the 1934 Bihar Nepal M_w 8.1 earthquake (*6*), which produced high-intensity shaking that was experienced throughout east Nepal and bordering regions of India (Fig. 1). To confirm the absence of rupture associated with this event and determine which events have led to the tectonic scarps, we conducted a paleoseismic study across the Himalayan front in the Marha Khola region, southeast of Kathmandu, in an area close to the inferred 1934 rupture zone.

Since ~20 million years ago, the deformation front resulting from the India/Asia collision has been expressed through the activation of two major thrust zones that are presumed to branch upward from a major midcrustal decollement: the Main Himalayan Thrust (*7*–*10*) (Fig. 1). In front of the rising Himalayas, thin-skinned thrust faulting has incorporated Cenozoic molasse deposits (Siwalik Formations) into the hanging walls of thrust faults, now expressed as the low-relief Siwalik Hills at the southern edge of the range. Geomorphic evidence of active tectonics indicates that 50 to 100% of the shortening across the Himalayas is transferred toward the southernmost of these faults, the Main Frontal Thrust fault (*2*, *5*, *11*). However, geodetic observations (*12*, *13*) indicate that current interseismic deformation is centered on a belt of microseismicity (*9*) that follows the southern edge of the Tibetan Plateau, ~100 km north of the frontal structure (Fig. 1). One explanation of this apparent paradox proposes that the current deformation mostly accumulates elastically at the transition along the decollement from steady creep beneath southern Tibet to locked beneath the High Himalaya, and that this elastic deformation releases and transfers to the front during large earthquakes (*2*, *9*), possibly like the 1934 M_w 8.1 earthquake.

[1]Laboratoire de Géodynamique des Chaînes Alpines, BP53, 38041 Grenoble, France. [2]California State University, Northridge, CA 91330, USA. [3]Seismolab, Department of Mines and Geology, Lainchaur, Kathmandu, Nepal. [4]Earth Consultants International, Tustin, CA 92780, USA.

*These authors contributed equally to this work.
†To whom correspondence should be addressed. E-mail: jlave@ujf-grenoble.fr